DOI: 10.31534/engmod.2022.2.ri.03a
Preliminary communication
Received: 22.02.2022.

Unconstrained Dynamic Simulation on Offshore Dual Derrick

Alaa Dandash(1,2,*), **WenSheng Xiao**(2), **HuaLin Liao**(1)

(1) *School of Petroleum Engineering, China University of Petroleum (East China), Qingdao, Shandong, 266580, CHINA*

(2) *College of Mechanical and Electronic Engineering, China University of Petroleum (East China), Qingdao, Shandong, 266580, CHINA*

(*) *corresponding author, Alaa Dandash, e-mail: alaa.dandash@live.com*

SUMMARY

With the increase in demand for oil and oil products, the petroleum industry is faced with the requirement for more complex tools to increase production at lower prices. The complexity of drilling tools is manifested in the complex geometry, fabrication, assembly, deformations, stresses and loads acting on them. This study introduces a dual derrick simulation procedure in a marine environment which provides a step towards a better understanding by giving a simulation close to the real state. The derrick was considered in equilibrium, and then the derrick vibration was simulated using field data in order to obtain stress distribution. This implies that the derrick can move freely and cause deformations in all directions without constraints. In this paper, the finite element method was employed to simulate the derrick in a static state and in motion, and then the obtained stress distribution was compared for both cases. A literature review on the analysis of environment working conditions is provided. The results showed that the vibration of the platform increased the stress considerably. The maximum combined stress increased by 27 %, while the maximum bending stress increased by 40 % and reached considerably higher values in the beams connected to the top of the derrick.

KEYWORDS: *Dual-derrick; offshore drilling; simulation; structural analysis; transient analysis.*

1. INTRODUCTION

The dual derrick is a drilling tower (mast) mounted on floating offshore platforms and used to reinforce drilling operations in remote locations. By holding two separate drilling groups, the dual derrick helps to reduce the drilling time and improve the efficiency of drilling operations.

Simulation methods used to obtain characteristics such as natural frequencies and mode shapes, design assessment and safety, and vibration response are becoming more popular and useful for performing studies on the derrick [1-6]. Due to the complex conditions of marine environments [7-9], extensive research is needed to understand the nature of loads acting on structures operating in the marine environment [10,11]. The derrick is a lattice structure, hence, various approaches such as mathematical approaches [12], experimental approaches [13], and simulation approaches are used to evaluate stress and loads acting on its structure.

In this paper, the simulation approach is selected to overcome the costs of the experimental approach and the instability of the mathematical approach.

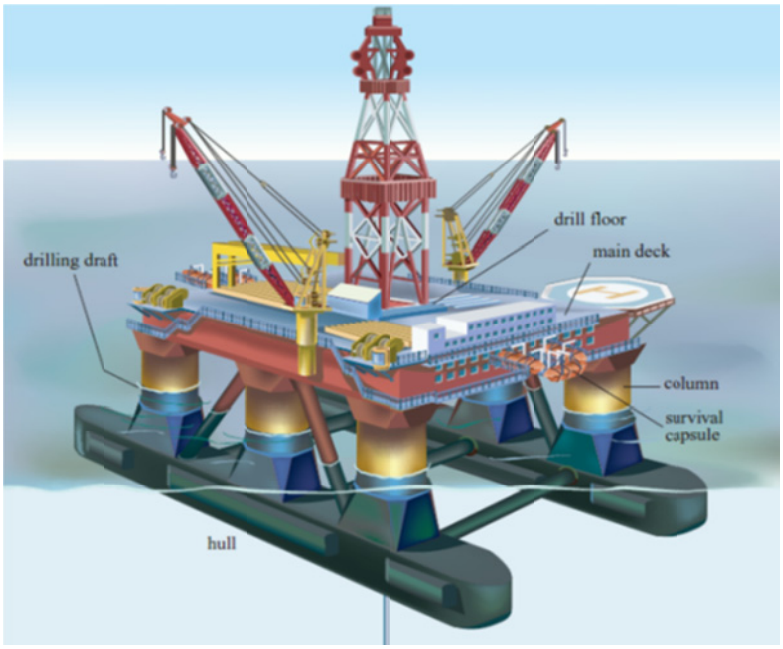

Fig.1 *Graphic illustration of a semi-submersible drilling rig with the derrick structure mounted on the drill floor*

1.1 THEORETICAL ANALYSIS OF THE MARINE ENVIRONMENT

Offshore platforms always operate in complex conditions, mainly caused by wind and waves [14]. According to [15], the impact of waves on semisubmersible may result in long-term direct structural damage or fatigue damage, characterized by nonlinearity. In a short-term sea state, the statistical characteristics of waves can be fully defined using Power Spectra Density (PSD) functions [16]. The fatigue life may be calculated based on the S-N fatigue approach assuming linear cumulative damage. These effects are not limited to the platform only, but damage the tools equipped on the platform [17,18]. Therefore, it is quite important to understand the combined wind/wave action [19,20]. Sea waves are formed by the interaction between wind and the sea surface, with the wind being the main energy source [16,21]. Most commonly occurring waves in ocean environments are due to winds which in different stages generate waves as the capillary, sea, and swell waves. The magnitude of a wave forming wind depends on the wind speed, wind duration and reach (the distance of water over which the wind blows). The state of these waveforms defines a random sea state for which the stochastic analysis approach is basically applied [22]. The wind velocity profile has an exponential character [23,24]:

$$V_z = V_{ref}\left(\frac{H}{H_0}\right)^a \tag{1}$$

Where V_z and V_{ref} are the average wind velocities at the height of H and H_0; and a is related to geomorphologic features.

According to [14], irregular water waves are mostly disturbed by winds in accordance with a logarithm profile, the governing equations are written as:

$$\sum_{j=1}\frac{\partial \hat{u}_j}{\partial t}+\bar{u}\sum_{j=1}\frac{\partial \hat{u}_j}{\partial x}+\frac{\partial \hat{u}_j}{\partial z}\sum_{j=1}\hat{w}_j=-\frac{1}{\rho_1}\sum_{j=1}\frac{\partial P_j}{\partial x} \tag{2}$$

$$\sum_{j=1}\frac{\partial \hat{w}_j}{\partial t}+\bar{u}\sum_{j=1}\frac{\partial \hat{w}_j}{\partial x}=-\frac{1}{\rho_1}\sum_{j=1}\frac{\partial P_j}{\partial x} \tag{3}$$

$$\sum_{j=1}\frac{\partial \hat{u}_j}{\partial z}+\sum_{j=1}\frac{\partial \hat{w}_j}{\partial x}=0 \tag{4}$$

Where $\hat{u}$ and $\hat{w}$ are x-direction and y-direction disturbed velocities, respectively; $\bar{u}$ is mean velocity in x-direction; j the order of the Stokes waves, ρ_1 air density; P pressure over wave surface. Equations 2-4 can be used to obtain the transferring energy E_j. Then, the relationship between the wave Power Spectral Density S_{waves} and the transferring energy E_j can be expressed as follows [14]:

$$\rho_2 g S_{waves}\left(\omega_j\right)=2\pi\frac{E_j}{\omega_j^2} \tag{5}$$

where ρ_2 is water density; ω is the wave frequency.

The IEC (International Electrotechnical Commission) Kaimal spectral equation can be used to model the wind (PSD) as [18]:

$$S(f)=\frac{4LV_0x^2}{\left(1+6fL/V_0\right)^{5/3}} \tag{6}$$

Where f is the wind frequency; x is the standard deviation of velocity component; L is the integral scale parameter of velocity component; and V_0 is the average wind velocity at the height of 10 meter above sea surface level.

The wave Power Spectral Density S_{waves} (PSD) can be derived by [14,18]:

$$S_{waves}(\omega)=\sqrt{\rho_1/2\rho_2 g^2}\cdot V_0\varpi^{3/2}\cdot\beta_1(\varpi)^{1/2}\cdot A(\varpi)\cdot\gamma \tag{7}$$

Where ϖ is the modified wave frequency; β_1 is the energy transfer coefficient; $A(\varpi)$ is the wave amplitude; γ is the peak adjusting coefficient, ρ_2 is water density.

According to [25], using the basic principle of proper orthogonal decomposition (POD), the time series of wind/waves can be expressed as:

$$\{y(t)\}=[\phi]\{a(t)\} \tag{8}$$

Where $y(t)$ is time series of wind or waves; $a(t)$ is a matrix of time principle coordinate; and $[\phi]$ is a POD mode matrix of a covariance matrix which is expressed as [26]:

$$[C][\phi]=\lambda[\phi] \tag{9}$$

Where $[C]$ is a covariance matrix; λ is the corresponding eigenvalues, where λ's value and quantity determine the energy related to the POD modes, and:

$$[C]=\left[R(0)\right]=\int\left[S(\omega)\right]d\omega \tag{10}$$

Where $[R]$ is a correlation matrix; and $\left[S(\omega)\right]$ is the PSD matrix [26].

Solving the aforementioned equations, the low-order PSD matrix $\left[\hat{S}(\omega)\right]$ is expressed as [26]:

$$\left[\hat{S}(\omega)\right]=[\phi]^T\left[S_a(\omega)\right][\phi] \tag{11}$$

Here, $\left[S_a(\omega)\right]$ is the PSD matrix related to $a(t)$.

Other methods for decomposing the wind/wave signal can be used as wavelet packet transform [27] or convolution wavelet packet transform [28].

Generally speaking, the Bernoulli equation is used to calculate wave forces [22]:

$$\int\frac{\partial V}{\partial t}dS+\frac{P}{\rho_w}+gz+\frac{V^2}{2}=f(t) \tag{12}$$

where ρ_w is the water density. The function $f(t)$ here expresses the dynamic boundary condition at the wave surface where the pressure is zero; and gz is the hydrostatic pressure at the free surface produced by waves. According to [22], the total water pressure at any point is expressed as:

$$P_{tot}=-\rho_w\left(gz+\int\frac{\partial V}{\partial t}dS+\frac{V^2}{2}\right) \tag{13}$$

The dynamic pressure P at any point is related to water element acceleration and velocity. In terms of the velocity potential function Φ, it can be written as [22]:

$$P=-\left(\rho_w\frac{\partial\Phi}{\partial t}+\frac{\rho_w}{2}\left[\left(\frac{\partial\Phi}{\partial x}\right)^2+\left(\frac{\partial\Phi}{\partial z}\right)^2\right]\right) \tag{14}$$

According to [29], the Morison's equation is defined as a distributed wave force per unit length of the structure in the normal direction:

$$f_m=C_D|v|v+C_M\dot{v} \tag{15}$$

where C_D expresses the hydrodynamic drag force influence; C_M expresses the mass force influence; v is the velocity components of water at the wave-free surface; and $\dot{v}$ is the acceleration components of water at the wave-free surface.

For a cylindrical member, as defined in [22,29]:

$$C_D=0.5\,D\,\rho_w c_d \tag{16}$$

$$C_M=0.25\pi D^2\rho_w c_m \tag{17}$$

where D is the diameter of the cylindrical member, ρ_w is the density of water, c_d and c_m are the drag and mass force coefficients of Morison's equation, respectively.

The above analysis enables an estimation of the offshore structure state of motion based on spectral analysis of the wave sea state.

For most problems of structural dynamics of a mechanical system, the spatial discretization for the principle of virtual work using the finite element method gives the semi-discrete finite element equation of motion as follows [30]:

$$[M]\{\ddot{u}\}+[C]\{\dot{u}\}+[K]\{u\}=\{F(t)\} \tag{18}$$

in which $[M]$ is the structural mass matrix; $[C]$ is the damping matrix; $\{\ddot{u}\}$ is the nodal acceleration vector; $\{\dot{u}\}$ is the nodal velocity vector; $\{u\}$ is the nodal displacement vector; $[K]$ is the stiffness matrix; $\{F(t)\}$ is the applied load vector [14,15]. The damping matrix $[C]$ is determined by the following equations [30]:

$$[C]=\alpha[M]+\beta[K] \tag{19}$$

where α and β are the constants in Rayleigh damping [30].

This paper provides a simplified unlimited simulation procedure for simulating the derrick in motion. Generally speaking, the procedure to be followed in performing such as simulation depends on given instructions such as providing fixed supports or limited directions or points. However, in this paper, no fixed supports or restrictions are used. The simulation procedure followed in this research brings the derrick to equilibrium conditions using vertical loads. To capture the impact of motion, characteristics of the platform's motion are modelled using rotational velocity, linear velocity, and rotational acceleration features; based on field data from the South China sea estimated from [6]; to obtain a simulation close to reality. The distribution of direct stress, maximum combined stress, and maximum bending stress was analysed using this procedure which emphasized the complexity of stress distribution and the stress concentration locations.

2. SIMULATION PROCEDURE

The derrick model was built in ANSYS WORKBENCH, using DESIGN MODELER (DM). The main points of the derrick are created in a text form using a notepad. The points are then imported to DM from the points file. Beams, columns, and bracing members are first formed in linear shape and then a cross-section of the I-beam is assigned to these members. The base is created using the surface feature and a surface thickness is assigned to the surface. This base is used to model the motion of the platform. The model created in (DM) is then transferred to the mesh cell in STATIC STRUCTURE, MECHANICAL.

Structural steel with a density of 7850 Kg/m^3 and tensile yield strength of 2.5e8 Pascal was assigned to create the structure of the derrick. The joints between different members are assumed as fixed joints, as shown in Figure 2a.

The next step is meshing, the mesh generator used a mechanical mesh type to produce (55882) elements, starting from (82284) nodes. The static analysis is performed considering the maximum design loads in the two drilling centres while fixed support is assigned to the base. After performing the static analysis, the model is transferred from the mesh cell in the static block to the mesh cell in the transient block, which transfers the mesh and joints created previously, but no loads or results are transferred.

Three vertical forces are applied, as depicted in Figure 2b. Two forces (C, E) represent the maximum design vertical loads acting downwards in both drilling centres, and one vertical load (F) acting upwards represents the buoyancy force. These three loads create an equilibrium condition, i.e. the structure cannot move, according to Newton's laws of motion, the vibration and translation of the derrick are modelled using rotational velocity (A), linear velocity features (D), and rotational acceleration (B) feature are applied as in Figure 2b. The

derrick in this study is considered to be shielded so that the wind forces acting directly on the derrick are not presented.

Setting the derrick conditions in motion: In this paper, representative characteristics of the platform's motion are used to simulate the motion of the derrick, including rotational velocity, rotational acceleration, linear velocity, and vertical forces. Rotational velocity expresses the movement of the derrick (platform) in terms of rotations around the rotation axis. It is set as a tabular value, where three components of rotations are used to describe this motion. The rotational acceleration is applied to all bodies around the rotation axis. Linear velocity expresses the linear movement of the derrick (platform) in the vertical direction. Vertical forces include maximum design load, wave loads, drilling loads, and any other vertical loads that might act upon the derrick such as compensators, and Top Drive System (TDS) loads. This paper considers the maximum design load on one side, and the wave and current loads transferred to the derrick through the platform on the other side. No restrictions on the structure movement are applied in order to have an unconstrained simulation.

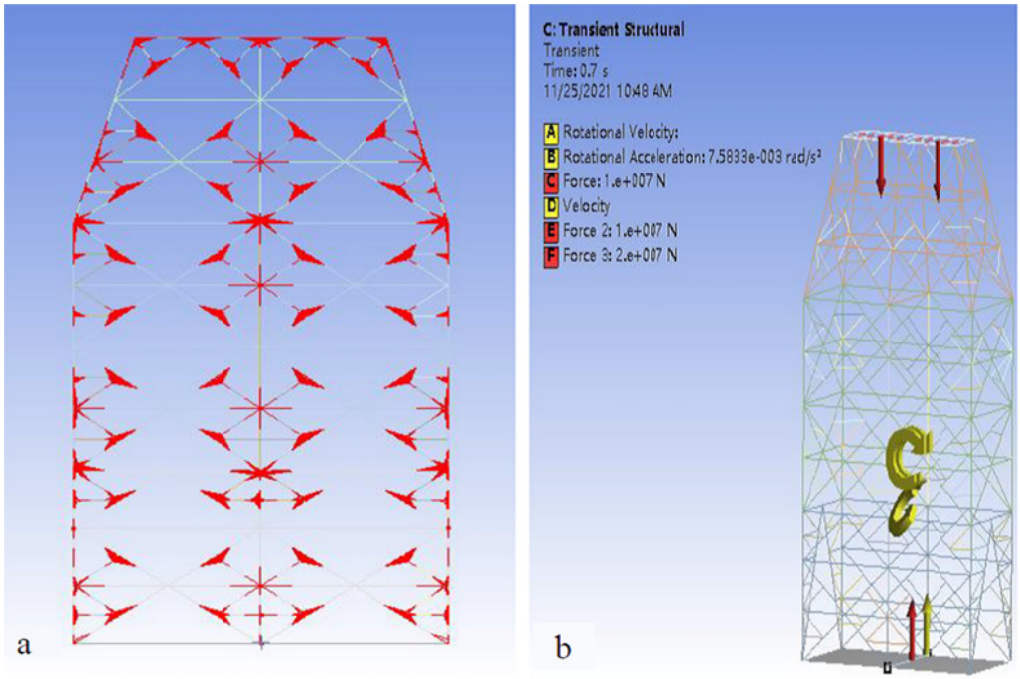

Fig. 2a *(to the left) shows the connections between the derrick members*

Fig. 2b *(to the right) shows the derrick conditions under simulation. A: rotational velocity; B: rotational acceleration; C: vertical force represents the maximum vertical load in the first drilling centre; E: vertical force represents the maximum vertical load in the second drilling centre; D: linear velocity of the derrick in the vertical direction; F: vertical force acting on the base to create the equilibrium conditions of the derrick*

3. RESULTS AND DISCUSSION

The dual derrick model was built in ANSYS (DM) using beams, columns, and the secondary bracing system. A structural steel material was assigned for the derrick model. Static and Transient analyses of the loads (Maximum vertical design loads) acting on the derrick were performed. The transient analysis was performed over eight seconds of time to perform one full cycle of platform vibration, which is close to the timing in real-life conditions. This section

presents and compares the direct stress, maximum combined stress, and maximum bending stress induced by the maximum vertical load in a stationary state and in motion. The results show that the movement of the derrick (platform) significantly increased the stress caused by vertical loads, and highlight the complexity of stress distribution.

Figure 3 illustrates the direct stress results from static and transient analysis, respectively. The results agree that the highest value of direct stress was observed at the same location, in secondary bracing members connected to the middle main leg with an increment of *11 %* related to the motion of the derrick.

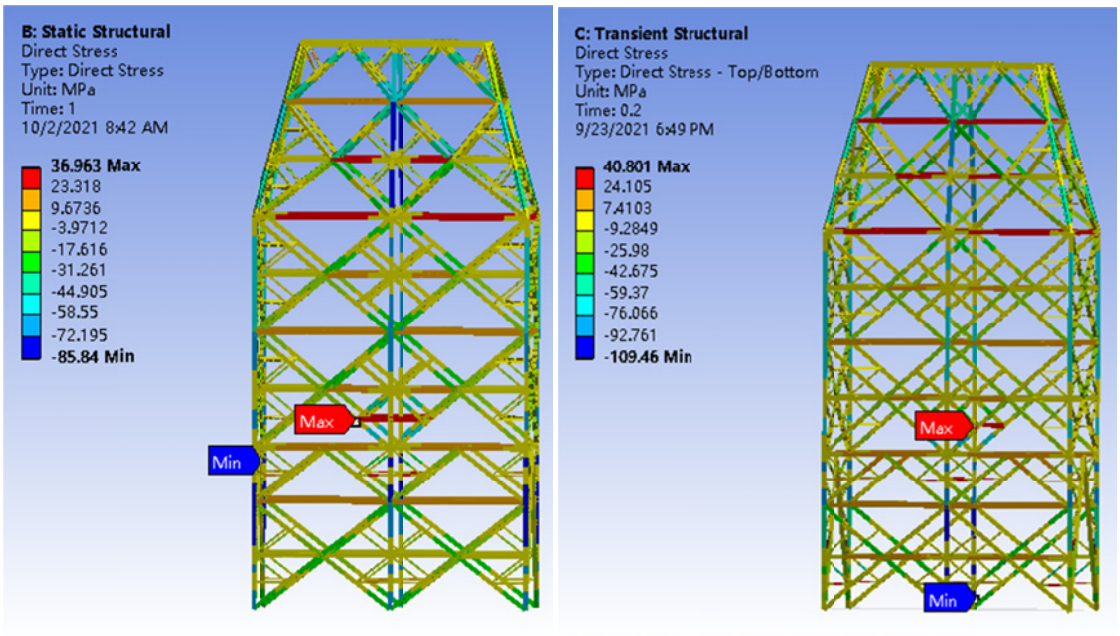

Fig. 3 *Direct stress distribution in the dual-derrick resulted from static analysis (to the left) and transient analysis (to the right) - unit (. e6 Pascal)*

Taking the maximum values of combined stress and comparing the results as depicted in Figure 4 show that the motion of the derrick (platform) increased the stress induced by vertical loads considerably. The results showed that the maximum combined stress induced in the derrick increased by *27 %* due to the platform motion.

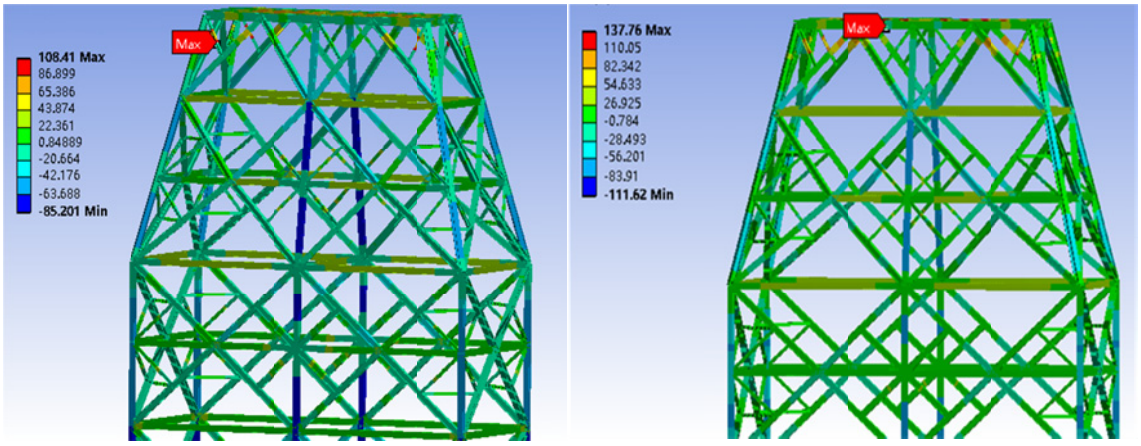

Fig. 4 *Maximum combined stress distribution in the dual-derrick resulted from static analysis (to the left) and transient analysis (to the right) - unit (. e6 Pascal)*

The maximum bending stress reached considerably high values in the beams connected to the top of the derrick, as stated in Figure 5, where the highest bending stress reached 110.e6 Pascal and 153.e6 Pascal for static and transient analysis, respectively, with an increment of *40 %* corresponding to the platform motion. Meanwhile, the stress distribution is almost the same in both cases.

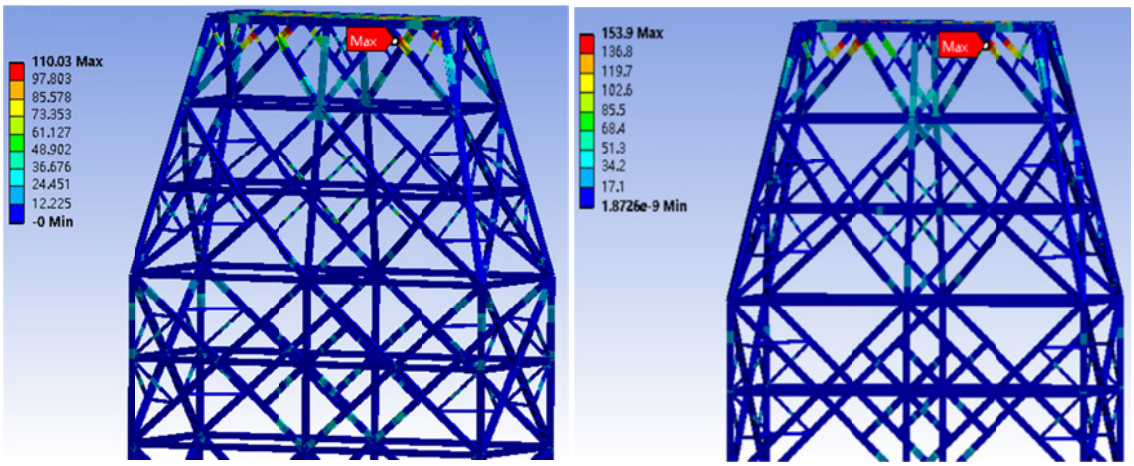

Fig. 5 *Maximum bending stress distribution in the dual-derrick resulted from static analysis (to the left) and transient analysis (to the right) - unit (. e6 Pascal)*

The results presented in Figures 3-5 highlight the complexity of the stress distribution in the derrick structure. The results of the simulation agree with the results obtained by [14] since the stresses of the derrick under fluctuating wind and waves are higher near the deck and on the top of the derrick.

4. CONCLUSIONS

This paper presented a static and transient analysis for an offshore dual derrick, to detect the stress produced by the maximum vertical design loads. The main goal of this study was to achieve a simulation of the derrick during movement closer to a real-life situation and to record the resulting stress distribution. The derrick model was studied in the stationary state and in motion. The motion study considered the rotational velocity, rotational acceleration and linear velocity in the vertical direction. The static and transient calculations highlighted the complexity of stress distribution in both stationary and in motion. The results showed that the stress increased considerably under the effect of motion. The maximum combined stress increased by *27 %*, while the maximum bending stress increased by *40 %*. The highest stress value was located in the bracings connected to the top of the derrick, and it corresponds to maximum bending stress. This emphasises the need for more attention to this area the during design and assessment process.

5. DECLARATION

The authors confirm that the article has no conflicts of interest. The results of this study should not be used for any industrial purposes. The authors are not responsible for any damage and/or any loss caused by the misuse of the results of this paper.

6. REFERENCES

[1] J. Pei, S. Deng, G. Chen, et al. Mechanical performance analysis of petroleum derrick substructure, *Applied Mechanics and Materials*, Vol. 105, pp. 2121-2124, 2011.

https://doi.org/10.4028/www.scientific.net/AMM.105-107.2121

[2] J. Hu, Y. Tang, S. Li, Vibration test and assessment for an ocean drilling rig derrick: Taking the ZJ50/3150DB drilling rig as an example, *Petroleum Exploration and Developmen*t, Vol. 40, No. 1, pp. 126-129, 2013.

https://doi.org/10.1016/S1876-3804(13)60014-2

[3] F. Guan, C. Zhou, S. Wei, et al. Load-carrying capacity analysis on derrick of offshore module drilling rig, *The Open Petroleum Engineering Journal*, Vol. 7, No. 1, pp. 29-40, 2014. https://doi.org/10.2174/1874834101407010029

[4] C. Wang, Z. Xu, L. Xiang, et al. Dynamic response analysis of ocean drilling derrick under the dynamic load, *Advanced Materials Research*, Vol. 977, pp. 387-390, 2014.

https://doi.org/10.4028/www.scientific.net/AMR.977.387

[5] J. Zeng, G. Chen, J. Mo, et al. Derrick structure design and finite element analysis of CPOE-16 jack-up, ASME 2014 33rd International conference on ocean, offshore and arctic engineering, San Francisco, California, USA, June 8- June 13 2014, Paper no. V04AT02A006. https://doi.org/10.1115/OMAE2014-23099

[6] G. Zhao, D. Liu, W. Wang, et al. Numerical simulation study on the stability of K-type derrick for deep-water drilling rigs, *Journal of Southwest Petroleum University* (science and technology edition), Vol. 39, pp.1-7, 2017. (In Chinese)

http://www.xml-data.org/XNSYDXXBZRB/HTML/2017-3-158.htm

[7] S. Gomathinayagam, C.P. Vendhan, J. Shanmugasundaram, Dynamic effects of wind loads on offshore deck structures - A critical evaluation of provisions and practices, *Journal of Wind Engineering and Industrial Aerodynamics*, Vol. 84, No. 3, pp. 345-367, 2000.

https://doi.org/10.1016/S0167-6105(99)00113-0

[8] G. Zhai, Z. Ma, Z. Hang, The wind tunnel tests of wind pressure acting on the derrick of deepwater semi-submersible drilling platform, Proc. 2011 2nd International conference on advances in energy engineering (ICAEE 2011), Bangkok, Thailand, December 27-December 28 2011, pp. 1267-1272. https://doi.org/10.1016/j.egypro.2011.12.1087

[9] G. Ross, R.D. Beck, T. Jennings, et al. Wind testing of a dual derrick, Proc. Offshore Technology Conference, Houston, Texas, USA, May 6 - May 9 2013, Page no. OTC 24262.

https://doi.org/10.4043/24262-MS

[10] A. Kareem, Wind induced response analysis of tension leg platform, *Journal of Structural Engineering*, Vol. 111, No. 1, pp.37-55, 1985.

https://doi.org/10.1061/(ASCE)0733-9445(1985)111:1(37)

[11] A. Kareem, T. Kijewski, C.E. Smith, Performance analysis and performance of offshore platforms in Hurricanes, *Wind and Structures*, Vol. 2, No. 1, pp. 1-23, 1999.

https://doi.org/10.12989/was.1999.2.1.001

[12] A. Kassimali, Three-dimensional framed structures. In: *Matrix Analysis of Structures*, Second edition, Cengage Learning, Southern Illinois, USA, pp. 417-498, 2012.

[13] P. Hu, Dynamic characteristic research of T-derrick on floating drilling platform, Master thesis, College of Mechanical Engineering, China University of Petroleum (East China), Qingdao, China, 2011. (Thesis in Chinese)

[14] J. Ma, D. Zhou, Z. Han, et al. Fluctuating wind and wave simulations and its application in structural analysis of a semi-submersible offshore platform, *International Journal of Naval Architecture and Ocean Engineering*, Vol. 11, No. 1, pp. 624-637, 2019.

https://doi.org/10.1016/j.ijnaoe.2018.11.001

[15] R.G. Bea, Performance shaping factors in reliability analysis of design of offshore structures, *Journal of Offshore Mechanics and Arctic Engineering*, Vol. 122, No. 3, pp. 163-172, 2000. https://doi.org/10.1115/1.1287507

[16] L. Cui, J. Xu, et al. Fatigue analysis on key components of semi-submersible platform, Proc. ASME 2010 29th International conference on ocean, offshore and arctic engineering, Shanghai, China June 6– June 11, 2010. Paper no. OMAE2010-20973, pp. 671-675. https://doi.org/10.1115/OMAE2010-20973

[17] J. Ma, D. Zhou, Z. Ha, et al. Numerical simulation of fluctuating wind effects on an offshore deck structure, *Shock and Vibration J*, Vol. 2017, pp. 1-17, 2017.

https://doi.org/10.1155/2017/3210271

[18] J. Ma, D. Zhou, Y. Ba, et al. Fatigue assessment on local components of a semisubmersible platform subjected to wind and wave loads, *Journal of Vibroengineering*, Vol. 20, No. 2, pp. 989-1005, 2018. https://doi.org/10.21595/jve.2017.18872

[19] M. Philippe, A. Babarit, P. Ferrant, Aero-hydro-elastic simulation of a semi-submersible floating wind turbine, *Journal of Offshore Mechanics and Arctic Engineering*, Vol. 136, No. 2, 2014. https://doi.org/10.1115/1.4025031

[20] T.T. Tran, D.H. Kim, A CFD study of coupled aerodynamic-hydrodynamic loads on a semisubmersible floating offshore wind turbine, *Wind Energy*, Vol. 21, No. 1, pp. 70-85, 2018. https://doi.org/10.1002/we.2145

[21] A. Elshafey, M. Haddara, H. Marzouk, Estimation of excitation and reaction forces for offshore structures by neural networks, *Ocean Systems Engineering*, Vol. 1, No. 1, pp. 1-15, 2011. https://doi.org/10.12989/ose.2011.1.1.001

[22] H. Karadeniz, Water wave theories and wave loads, In: *Stochastic Analysis of Offshore Steel Sstructures*, Springer, London, UK, pp. 177-252, 2013.

https://doi.org/10.1007/978-1-84996-190-5_3

[23] K. Wang, T. Moan, M.O.L. Hansen, Stochastic dynamic response analysis of a floating vertical-axis wind turbine with a semi-submersible floater, *Wind Energy*, Vol. 19, No. 10, pp. 1853-1870, 2016. https://doi.org/10.1002/we.1955

[24] R. Hadzovic, M. Muratovic, B. Peros, New approach of determination dynamic wind load of the bora, Proc. 15th International research/expert conference, Prague, Czech Republic, 2011.

[25] X. Chen, A. Kareem, Proper Orthogonal Decomposition-Based Modeling, Analysis, and Simulation of Dynamic Wind Load Effects on Structures, *Journal of Engineering Mechanics*, Vol. 131, No. 4, pp. 325-339, 2005.

https://doi.org/10.1061/(ASCE)0733-9399(2005)131:4(325)

[26] J. Chen, R. Yang, R. Ma, Wind field simulation of large horizontal-axis wind turbine system under different operating conditions, *The structural design of tall and special buildings*, Vol. 24, No. 17, pp. 973-988, 2015. https://doi.org/10.1002/TAL.1221

[27] S.G. Mallat, A Theory for Multiresolution Signal Decomposition: The Wavelet Representation, IEEE Transactions on pattern analysis and machine intelligence, Vol. 11, No. 7, pp.674- 693, 1989. https://doi.org/10.1109/34.192463

[28] X. Zhao, B. Ye, Convolution wavelet packet transform and its applications to signal processing, *Digital Signal Processing*, Vol. 20, No. 5, pp. 1352-1364, 2010.

https://doi.org/10.1016/j.dsp.2010.01.007

[29] S.E. Abdel Raheem, Nonlinear behaviour of steel fixed offshore platform under environmental loads, *Ships and Offshore Structures*, Vol. 11, No. 1, pp. 1-15, 2016.

https://doi.org/10.1080/17445302.2014.954301

[30] Ansys tutorial. ANSYS FLUENT Tutorial Guide. Canonsburg, Pennsylvania, USA, 2017.